nature geoscience

SUPPLEMENTARY INFORMATION

https://doi.org/10.1038/s41561-018-0065-0

In the format provided by the authors and unedited.

# Widespread distribution of $OH/H_2O$ on the lunar surface inferred from spectral data

**Joshua L. Bandfield[1]*, Michael J. Poston[2,5], Rachel L. Klima[3] and Christopher S. Edwards[4]**

[1]Space Science Institute, Boulder, CO, USA. [2]Jet Propulsion Laboratory, California Institute of Technology, Pasadena, CA, USA. [3]Applied Physics Laboratory, Johns Hopkins University, Baltimore, MD, USA. [4]Northern Arizona University, Flagstaff, AZ, USA. [5]Present address: Southwest Research Institute, San Antonio, TX, USA. *e-mail: jbandfield@spacescience.org

# Supplementary Material to Widespread distribution of OH/$H_2O$ on the lunar surface inferred from spectral data, by J.L. Bandfield et al.

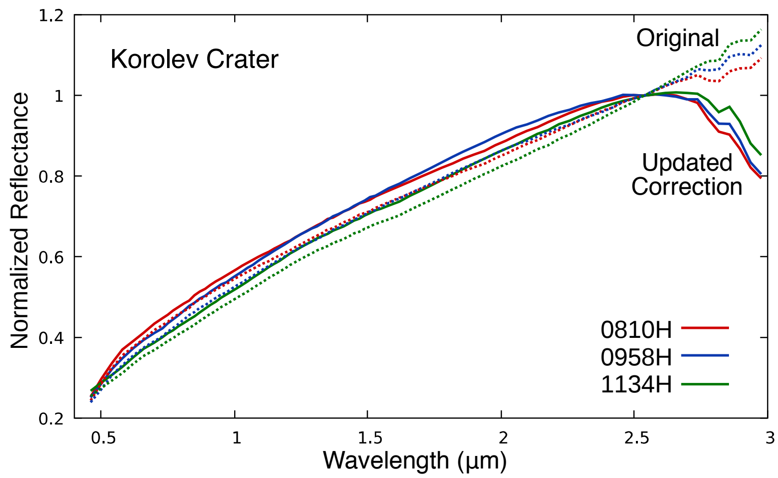


**Supplementary Figure S1.** Original (dashed lines) and updated (solid lines) $M^3$ thermally corrected spectra for a location within Korolev Crater acquired at local times from 0810H to 1134H. Although some variation is present in the updated correction spectra, the prominent 3µm absorption is present in all cases, even near local noon.

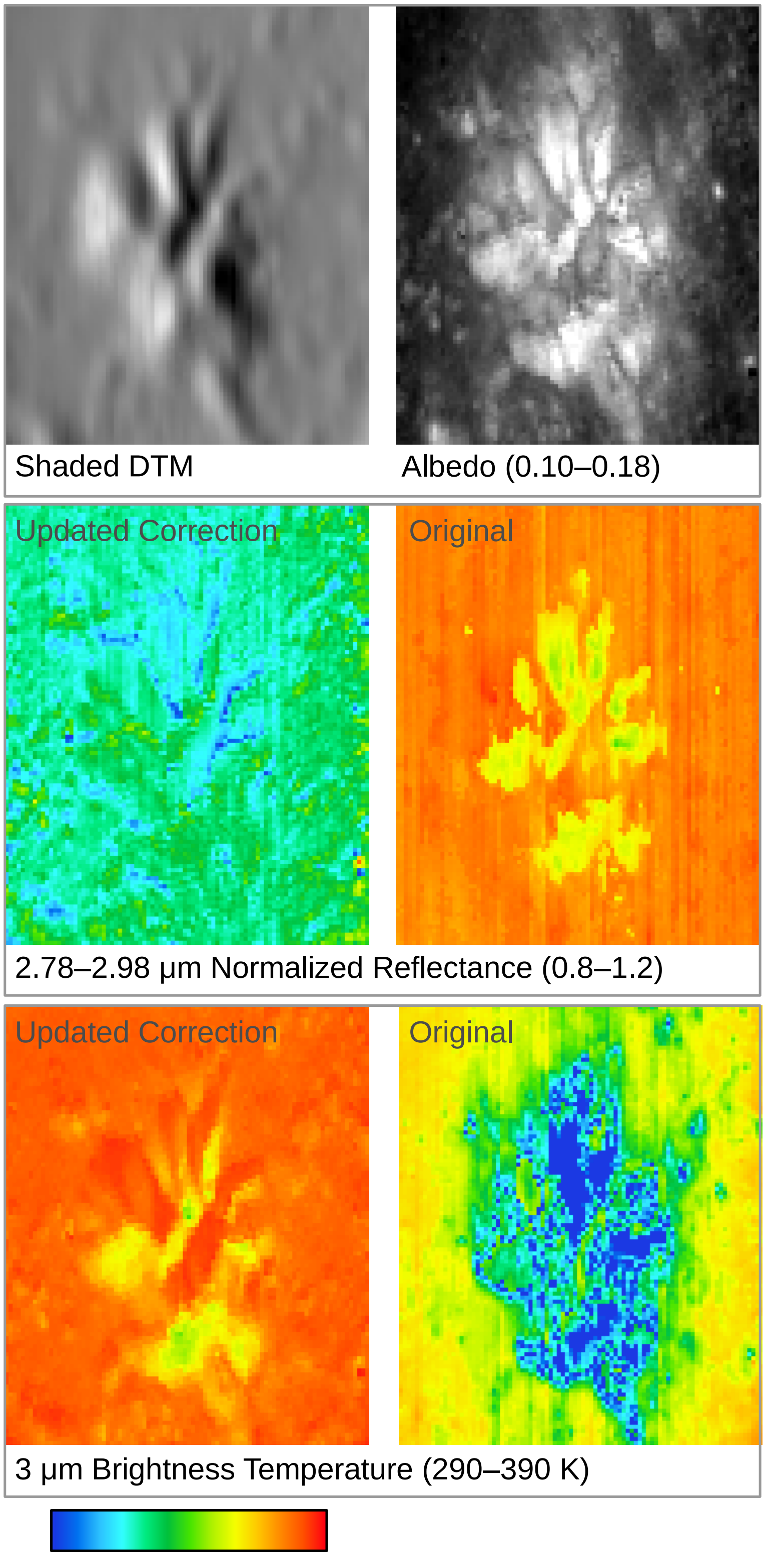


**Supplementary Figure S2.** Images covering the central peak and crater floor of Bullialdus Crater ($M^3$ image M3G20090610T070604; lines 15966–16074, samples 62–151). (top left) Shaded relief image derived from LOLA Kaguya digital elevation model. (top right) Broadband albedo used for the thermal emission and roughness modeling. (middle left and right) 2.78–2.98 μm reflectance normalized against 2.54 μm. The original data have a much shallower absorption with deeper features associated with higher albedo surfaces. The updated data (left) show similar spectral features, regardless of location, except artifacts caused by mis-registration of the topographic data with the $M^3$ data (linear blue features in the image). (bottom left and right) Derived 3 μm brightness temperatures (left) and surface temperatures (right) used for the thermal correction. The updated thermal model averages 46 K higher throughout the image, resulting in a much greater predicted thermal emission and deeper 3 μm spectral features.

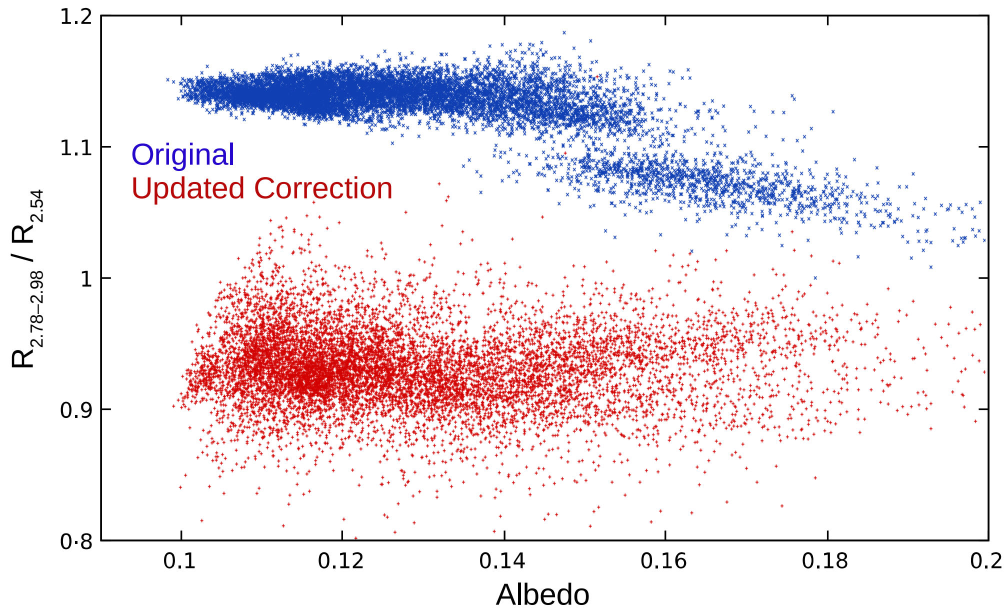


**Supplementary Figure S3.** Scatterplot showing the depth of the 2.78–2.98 μm absorption relative to surface albedo. The data are the same as shown in the middle images in Fig. S1. The original $M^3$ Level 2 thermally corrected data (blue) show a much shallower (or non-existent) 3 μm absorption with two distinct populations. The lower reflectance values that correspond to higher albedos are typically associated with the Bullialdus Crater central peak. This separate population disappears in the updated thermally corrected data (red; see also Fig. S1). The updated correction has a greater scatter due to imprecise registration between the topographic and the $M^3$ data. This results in errors in slope orientation that influence modeled surface temperatures and the resulting magnitude of the thermal correction.

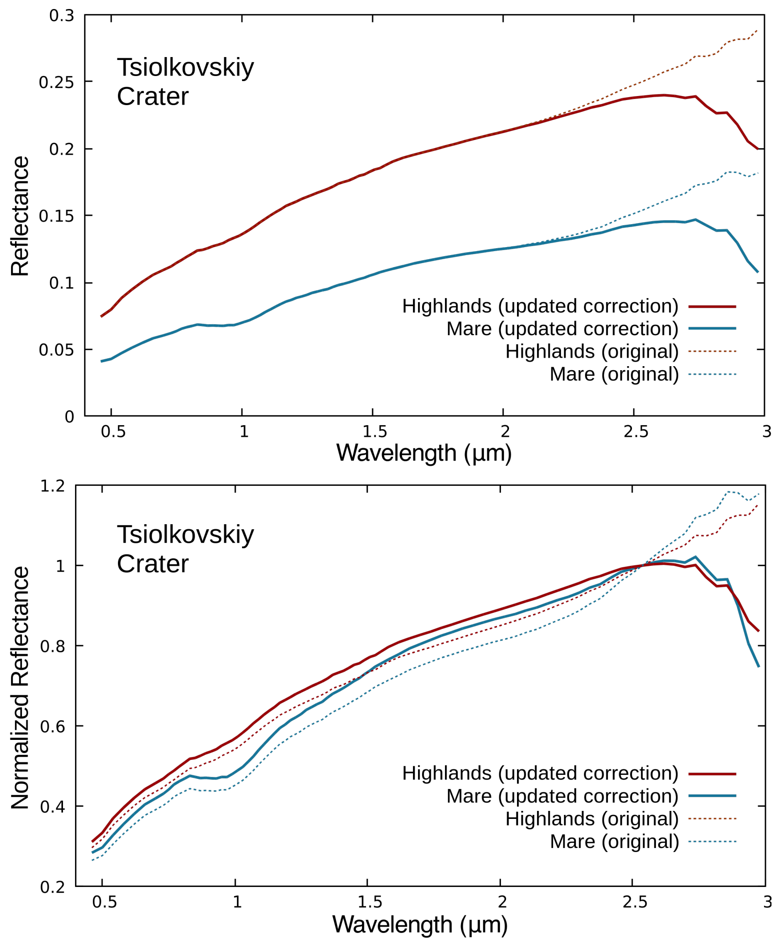


**Supplementary Figure S4.** Mare and highlands surface reflectance spectra within and near Tsiolkovkiy Crater. Mare surfaces have a slightly, but consistently deeper 3 μm absorption than adjacent highlands surfaces.

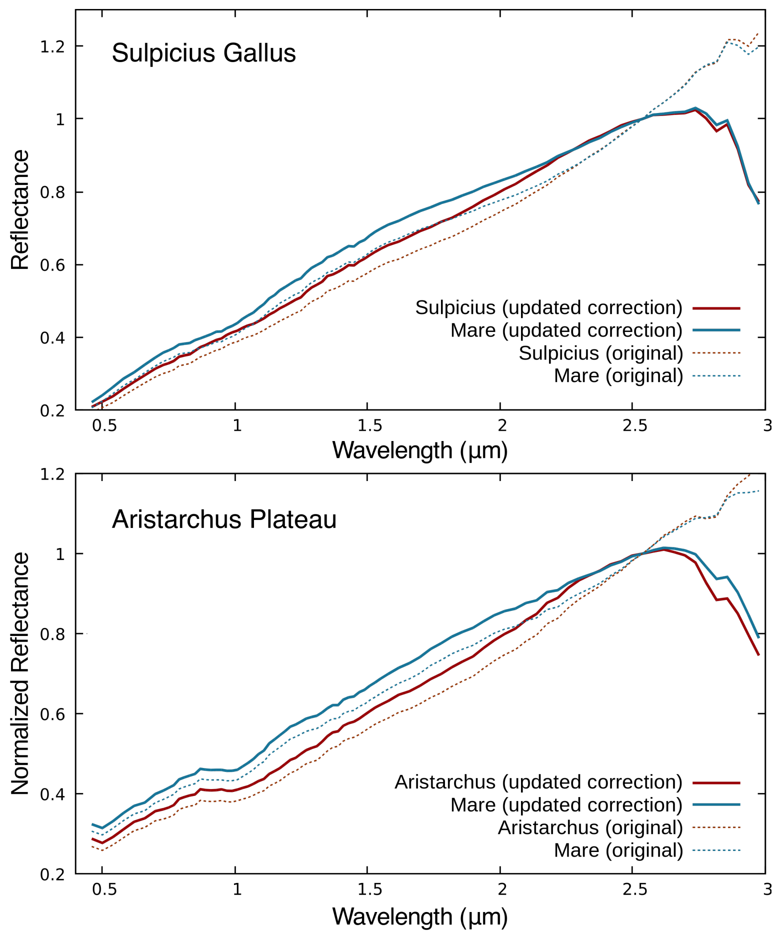


**Supplementary Figure S5.** Pyroclastic deposit surface reflectance spectra (red) compared with adjacent mare surface spectra (blue). Although some relative variation in the strength of the 3 µm absorption is present, there is no clear systematic difference between the two surface compositional types.

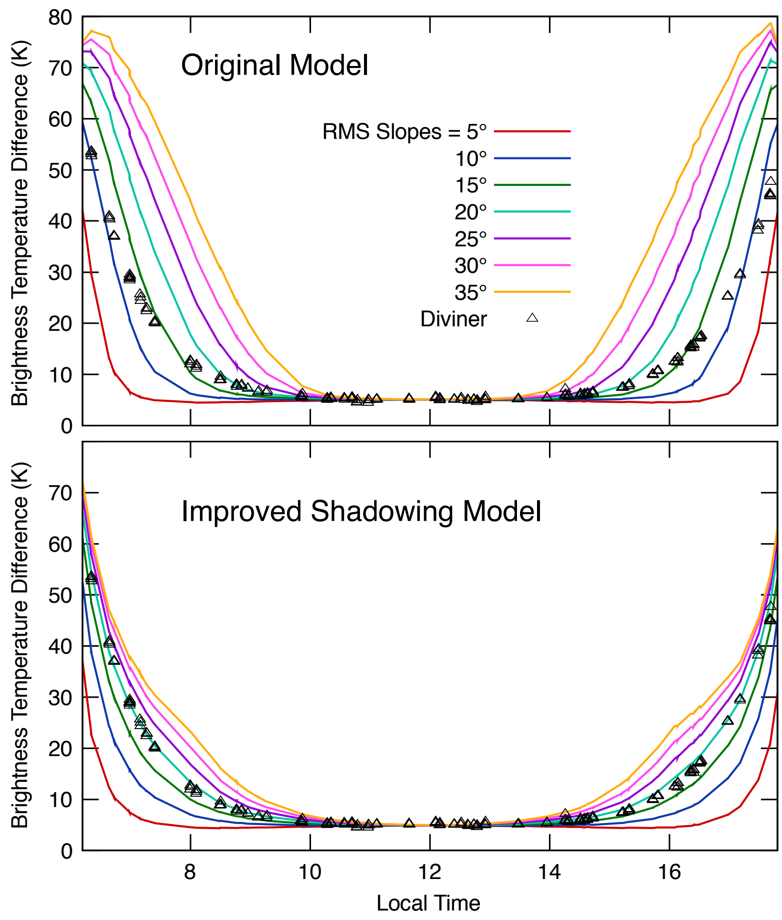


**Supplementary Figure S6.** Equatorial mare Channel 4 (centered near 8µm) minus Channel 7 (centered near 40µm) brightness temperature differences. The black triangles are the Diviner measurements and are the same data used in Bandfield et al. (2015)[10]. Colored lines show roughness thermal model results for a range of RMS slope distributions. The top plot shows the modeling used in previous work and the bottom plot shows the improved modeling used for this work. Data sensitivity to roughness becomes pronounced at solar incidence angles greater than ~30° (local times outside of 1000H to 1400H at the equator). The model matches the data at an RMS slope distribution of 20°, which is tha value used for this work. Small irregularities in the model lines are due to differences in solar distance between individual Diviner observations.

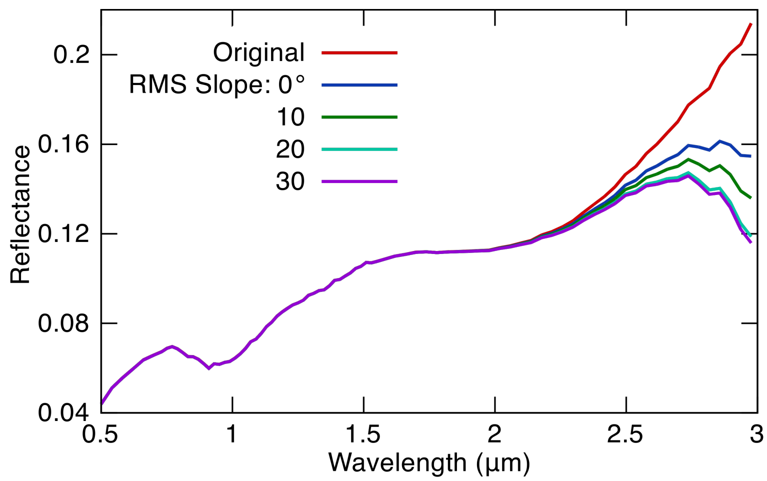


**Supplementary Figure S7.** Effects of surface roughness modeling on the thermally corrected $M^3$ spectra. At a solar incidence angle of 51°, surface roughness results and a wide variety of surface temperatures for sunlit and shadowed surfaces, resulting in a higher emitted radiance at short wavelengths near 3 µm. Removal of the excess emitted radiance results in a more prominent 3 µm absorption. The lunar surface is consistent with RMS roughness values of ~20°. The spectra shown here are from $M^3$ image M3G20090125T172601 and are the same data as that used in Fig. 1.

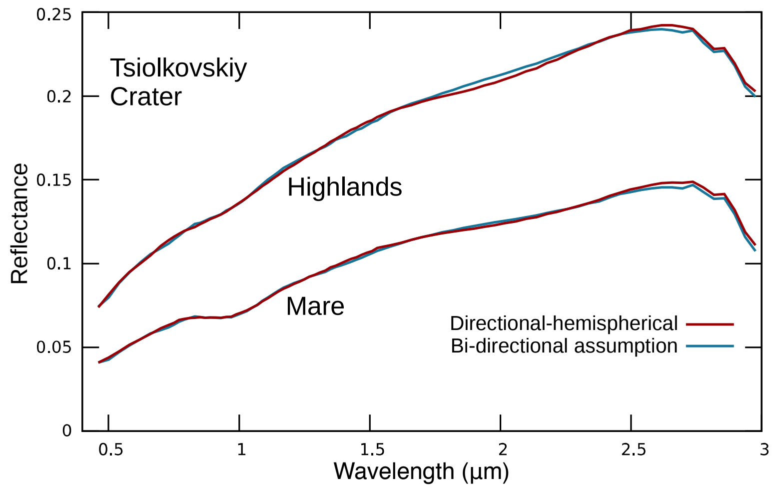


**Supplementary Figure S8.** Thermally corrected data from example mare and highlands surfaces (Fig. S4) showing the difference between using directional-hemispherical and bi-directional reflectance for emissivity determination for thermal removal. Although directional-hemispherical reflectance in this case is 9–14% higher than bi-directional reflectance, the resulting effect on emitted radiance and thermally corrected reflectance is small.

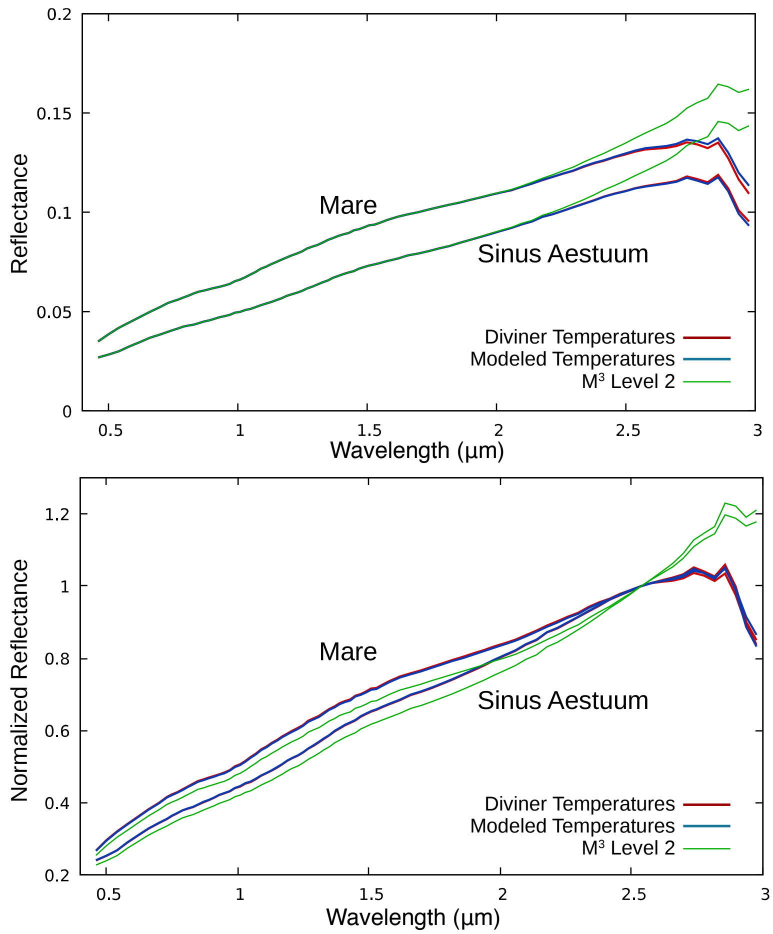


**Supplementary Figure S9.** Comparison of $M^3$ spectra corrected using temperatures derived from Diviner observations (red), the updated model (blue), and the original $M^3$ Level 2 thermally corrected spectra (green). Under the conditions of low solar incidence where anisothermality due to surface roughness is minimized, the modeled temperatures closely match the Diviner measurements and produce similar spectra with prominent 3 µm absorptions.

**Supplementary Table S1.** Image ID's, samples, line numbers, average geometry, and derived information for spectral plots shown in Figures 1, 2-4 and Supplementary Figures 2 and 3. All data were selected for surfaces with consistent and low slopes (<10°) to avoid potential mis-registration problems with the topographic data.

| Label | Samples | Lines | Original T(K) | Updated 3μm T(K) | Solar Incidence | Phase Angle | Albedo | Latitude (N) | Longitude (E) |
|---|---|---|---|---|---|---|---|---|---|
| **Aristarchus** | **M3G20090418T174554** | | | | | | | | |
| Aristarchus | 125-160 | 11770-11800 | 306.6 | 338.5 | 61.0 | 60.9 | 0.06 | 28.54 | 310.49 |
| Mare | 125-160 | 11001-11050 | 312.8 | 336.3 | 61.7 | 62.0 | 0.07 | 32.49 | 310.44 |
| **Sulpicius Gallus** | **M3G20090608T000122** | | | | | | | | |
| Sulpicius Gallus | 274-285 | 14065-14125 | 372.6 | 385.6 | 21.8 | 23.7 | 0.06 | 20.42 | 9.37 |
| Mare | 274-285 | 13351-13410 | 370.3 | 382.9 | 24.7 | 27.1 | 0.07 | 23.83 | 9.39 |
| **Gruithuisen** | **M3T20090418T020644** | | | | | | | | |
| On-dome | 54-64 | 10351-10360 | 0.0 | 332.2 | 62.9 | 54.3 | 0.13 | 36.72 | 319.32 |
| Off-dome | 54-64 | 10405-10435 | 301.5 | 339.5 | 61.4 | 54.1 | 0.08 | 36.10 | 319.30 |
| **Bullialdus Crater** | **M3G20090610T070604** | | | | | | | | |
| Central Peak | 100-105 | 15998-16003 | 16.3 | 376.3 | 17.7 | 23.3 | 0.18 | -20.71 | 337.68 |
| Crater Floor | 100-105 | 16095-16101 | 362.0 | 380.7 | 21.4 | 23.7 | 0.11 | -21.17 | 337.67 |
| **Reiner Gamma** | **M3G20090210T0330524** | | | | | | | | |
| Bright | 115-125 | 8960-8970 | 330.2 | 347.0 | 55.9 | 53.1 | 0.10 | 7.74 | 300.96 |
| Dark | 115-125 | 8871-8880 | 335.8 | 350.4 | 56.1 | 53.0 | 0.06 | 8.20 | 300.97 |
| **Mare Ingenii** | **M3G20090623T135841** | | | | | | | | |
| Bright | 18-24 | 3701-3708 | 351.8 | 369.4 | 35.2 | 37.2 | 0.12 | -33.73 | 162.78 |
| Dark | 18-24 | 3513-3520 | 359.0 | 374.6 | 34.2 | 36.6 | 0.07 | -33.06 | 162.78 |
| **Mare/Highlands** | **M3G20090529T183825** | | | | | | | | |
| Mare | 99-139 | 16888-16928 | 364.6 | 379.8 | 26.9 | 32.6 | 0.09 | -18.93 | 129.78 |
| Highlands | 99-139 | 16734-16773 | 314.8 | 370.2 | 28.7 | 32.0 | 0.16 | -18.19 | 129.78 |
| **Korolev Crater** | | | | | | | | | |
| 0800H (M3G20090814T102823) | 134-148 | 15667-15681 | 0.0 | 341.6 | 55.0 | 56.4 | 0.14 | -4.38 | 200.50 |
| 1000H (M3G20090718T014252) | 44-58 | 19200-19214 | 338.7 | 373.0 | 29.6 | 24.5 | 0.14 | -4.38 | 200.50 |
| 1200H (M3G20090620T181042) | 76-90 | 17948-17962 | 351.8 | 387.6 | 6.1 | 6.2 | 0.11 | -4.38 | 200.50 |
| **Sinus Aestuum** | **M3G20090609T183254** | | | | | | | | |
| Sinus Aestuum | 165-173 | 17154-17161 | 383.1 | 392.2 | 8.0 | 7.9 | 0.05 | 6.13 | 345.14 |
| Mare | 175-186 | 17692-17701 | 378.5 | 390.6 | 8.2 | 5.9 | 0.07 | 3.55 | 345.26 |
| **Solar Incidence Transect** | **M3G20090529T183825 (1-11) / M3G20090213T001153 (12-25)** | | | | | | | | |
| 1 | 176-189 | 12016-12027 | 353.1 | 385.0 | 11.5 | 14.8 | 0.13 | 4.35 | 130.33 |
| 2 | 121-141 | 11341-11360 | 349.5 | 382.2 | 15.0 | 18.4 | 0.14 | 7.53 | 129.85 |
| 3 | 106-117 | 11556-11569 | 353.1 | 381.4 | 18.5 | 19.9 | 0.13 | 6.51 | 129.67 |
| 4 | 7-23 | 15060-15077 | 346.8 | 379.8 | 19.9 | 32.5 | 0.13 | -10.24 | 128.79 |
| 5 | 54-66 | 16119-16133 | 346.5 | 378.0 | 24.3 | 32.9 | 0.12 | -15.28 | 129.23 |
| 6 | 184-190 | 17917-17924 | 319.6 | 370.7 | 30.8 | 33.9 | 0.15 | -23.83 | 130.45 |
| 7 | 212-227 | 18794-18813 | 312.0 | 368.9 | 33.2 | 36.6 | 0.14 | -28.05 | 130.81 |
| 8 | 207-215 | 19747-19757 | 301.2 | 364.2 | 37.4 | 41.1 | 0.14 | -32.61 | 130.75 |
| 9 | 46-58 | 20718-20730 | 279.4 | 359.1 | 42.6 | 50.7 | 0.13 | -37.31 | 129.03 |
| 10 | 91-98 | 21730-21740 | 18.1 | 353.5 | 46.1 | 53.5 | 0.14 | -42.15 | 129.47 |
| 11 | 125-137 | 22636-22650 | 4.7 | 343.9 | 50.7 | 56.4 | 0.17 | -46.51 | 129.90 |
| 12 | 88-95 | 18063-18070 | 0.0 | 343.0 | 54.1 | 53.6 | 0.18 | -4.86 | 263.11 |
| 13 | 211-230 | 16961-16980 | 31.9 | 340.9 | 56.9 | 63.4 | 0.13 | 0.75 | 263.72 |
| 14 | 191-210 | 12401-12420 | 0.0 | 338.2 | 58.4 | 64.7 | 0.13 | 24.10 | 263.62 |
| 15 | 171-190 | 10711-10730 | 0.0 | 330.5 | 62.7 | 65.6 | 0.13 | 32.74 | 263.50 |
| 16 | 151-170 | 8671-8690 | 0.0 | 321.0 | 67.5 | 67.7 | 0.13 | 43.16 | 263.35 |
| 17 | 161-180 | 7321-7350 | 1.1 | 316.7 | 69.6 | 71.2 | 0.12 | 50.02 | 263.39 |
| 18 | 33-39 | 9-13 | 0.0 | 309.0 | 70.1 | 80.3 | 0.18 | 87.30 | 245.25 |
| 19 | 121-140 | 3581-3600 | 0.0 | 308.3 | 71.9 | 77.3 | 0.15 | 69.13 | 262.63 |
| 20 | 216-235 | 6016-6035 | 0.0 | 307.4 | 72.9 | 77.9 | 0.14 | 56.70 | 263.88 |
| 21 | 101-120 | 4801-4820 | 0.0 | 298.2 | 77.0 | 72.9 | 0.13 | 62.90 | 262.62 |
| 22 | 69-78 | 682-690 | 0.0 | 289.9 | 77.8 | 81.1 | 0.19 | 83.94 | 257.41 |
| 23 | 91-110 | 2526-2545 | 0.0 | 288.2 | 80.2 | 78.0 | 0.14 | 74.51 | 261.71 |
| 24 | 65-80 | 745-760 | 0.0 | 281.6 | 80.8 | 80.8 | 0.18 | 83.60 | 257.68 |
| 25 | 26-45 | 1851-1870 | 12.1 | 275.1 | 84.0 | 75.3 | 0.14 | 77.96 | 259.52 |